Filtering Visible Light Reflections with a Single-Pixel Photodetector

Galisteo, Ander; Marcocci, Patrizio ; Zuñiga , Marco; Mucchi, Lorenzo; Guzman, Borja Genoves ; Giustiniano, Domenico

DOI
10.1109/SECON48991.2020.9158414

Publication date
2020

Document Version
Final published version

Published in
2020 17th IEEE International Conference on Sensing, Communication and Networking, SECON 2020

Filtering Visible Light Reflections with a Single-Pixel Photodetector

Ander Galisteo*†, Patrizio Marcocci‡, Marco Zuniga§,
Lorenzo Mucchi‡, Borja Genovés Guzmán* and Domenico Giustiniano*
*IMDEA Networks Institute, Madrid, Spain.
†Universidad Carlos III de Madrid, Spain.
‡Department of Information Engineering, University of Florence, Italy.
§Delft University of Technology, The Netherlands.
Email: ander.galisteo@imdea.org, patrizio.marcocci@unifi.it, m.a.zunigazamalloa@tudelft.nl,
lorenzo.mucchi@unifi.it, borja.genoves@imdea.org, domenico.giustiniano@imdea.org

***Abstract*—Light-based positioning systems (LPS) are gaining significant attention as a means to provide localization with cm accuracy. Many of these systems estimate the object position based on the received light intensity, and work properly in 'ideal' environments such as large open spaces without obstructions around the light-emitting diode (LED) and the receiver, where reflections are negligible. In more dynamic environments, such as indoor spaces with moving people and city roads with moving vehicles, materials cause a wide variety of reflections. This causes variations in the received light intensity and, as a consequence, gross localization errors in LPS. We propose a new multipath detection technique for improving LPS that does not require the knowledge of the channel impulse response and then, it is suited to be implemented in low-cost positioning receivers that use a single-pixel photodetector. To develop our technique, we (i) analyze the statistical properties of non-line-of-sight (NLOS) components, (ii) develop an automated testbed to study the reflections of different types of surfaces and materials, and (iii) design an algorithm to remove the NLOS components affecting the positioning estimate. Our experimental evaluation shows that, in complex environments, our methodology can reduce the localization error using LEDs up to 93%.**

***Index Terms*—Visible Light Communication, Localization, Reflections, Experiments.**

I. Introduction

Artificial lighting is everywhere, from the light bulbs on the ceilings to car headlights. It is expected that, by 2025, light-emitting diodes (LEDs) will account as 98% of the lighting [1]. This trend makes visible light communication (VLC) an attractive technology for data transmission and, more recently, for locating objects and people using light-based positioning systems (LPS). LPS are gaining significant attention from industry and the scientific community due to its high accuracy. Broadly speaking, LPS can be divided into two categories depending on the type of optical receiver they use: LPS relying on photodiode (PD) and LPS relying on image sensor (camera) [2–6]. PDs provide higher throughput and energy-efficiency than cameras, and thus, they are a better choice for wearable devices (low energy) and vehicular networks (high throughput). Image sensors are popular due to their widespread availability in smartphones, but they have a reduced data rate (only kb/s rather than Mb/s or more [7]) and a higher energy cost (∼300 mW rather than a few mW [8]).

The area of LPS for smartphones is relatively mature and there are products already in the market [9], whereas LPS in wearable devices and vehicular networks have encountered additional difficulties. Compared to cameras, the main constraint of PDs is its sensitivity to interference caused by optical reflections coming from the surroundings made of different type of surfaces and materials. All the incoming optical rays sum up at the PD due to operating as a single pixel [10]. This implies that reflections affect LPS that work with a single-pixel PD as receiver, because the majority of LPS relies on the received signal strength (RSS) resulting from all the light components [11]. Therefore, LPS relying on PD are affected by location errors (from a few cm to 1 m) in real deployments [10], [12–14]. Image sensors can instead solve optical interference by exploiting multiple pixels [15].

Discerning the line-of-sight (LOS) path for positioning using a single-pixel PD receiver is not easy. Estimating the channel impulse response (CIR) to infer the LOS and reflected non-line-of-sight (NLOS) paths requires a powerful analogue-to-digital converter (ADC) and high processing capabilities on the receiver side, which may not be available or desired [16]. Reflected paths have been ignored in recent experimental works for LPS relying on PD [2], [3], [17], [18], and reflections have been characterized only from a theoretical point of view [19–21]. However most of works are limited to simulations of simple static indoor scenarios [10], [12], [13], [22], [23] and the detection/discrimination of NLOS components has been done exploiting quite complex schemes as multiple sources [24] or multiple receivers [18], [25].

Against this background, this work presents a technique to discern and filter reflected light paths using a single-pixel PD. Our key idea is to avoid the need of the CIR knowledge and to propose a low-complexity practical approach based on time series of the RSS collected with a low-cost PD. This trade-off is possible in our scenarios of interest (vehicular or wearable networks) because (i) nodes are mobile, and thus,

Ander Galisteo and Patrizio Marcocci are both first authors of this work.

The work of Ander Galisteo was supported in part by the "La Caixa International PhD Program" Fellowship under Grant LCF/BQ/ES16/11570019.

978-1-7281-6630-8/20/$31.00 © 2020 IEEE

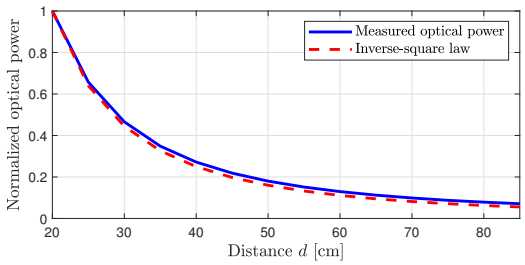

Fig. 1: Comparison of inverse-square law with respect to RSS measurements using low-cost PD receivers in ideal LOS links.

changes in reflection occur over a short period of time, (ii) the reflections from materials have unique statistical properties that can be exploited to filter out NLOS components, and (iii) our scenarios can accept some marginal delay, which allows us to work with short time series.

All in all, the main contributions of our work are:

- Section II: system model containing the motivation and a dedicated experimental testbed that allows making controllable and realistic down-scaled characterization of visible light multipath in low-cost receivers.
- Section III: a statistical method to identify and discriminate NLOS components with limited sampling rate of the receiver.
- Section IV: a decision tree algorithm that can run in low-cost receivers and that uses only two features, yet it can differentiate between different types of reflections.
- Section V: a new algorithm for removing NLOS components and an experimental evaluation that shows that our method can improve the accuracy of LPS up to 93%.

II. System Model

A. Accuracy of positioning techniques with reflected light

As stated before, positioning techniques with single-pixel PDs typically rely on RSS-based estimation algorithms. These solutions exploit the so-called *inverse-square law*, which characterizes the relation between distance and RSS in pure LOS scenarios as

$$\mathrm{RSS} \propto \frac{1}{d^2}, \tag{1}$$

where d is the distance between transmitter (TX) and receiver (RX). Figure 1 validates the application of the inverse-square law in VLC by comparing (1) to a simple, practical experiment where the optical received power is measured for multiple d values. This good match has been the foundation behind the uptake of LPS in the last few years [11]. However, the monotonic curve of Fig. 1 becomes less predictable and noisier if a fraction of the light does not reach the RX through the LOS link, i.e., it comes from reflected paths.

Since reflections are different for every reflector material, in order to quantify the impact of reflections, we first consider the ideal environment (considering only the LOS component), and subsequently, we include the presence of light reflected by different materials: shiny glass (glass), grey satin metal (metal), chipboard (rwood), plywood (swood) and foam core (wfoam). We use our experimental setup presented in Fig. 2 where the TX and the RX are at a fixed distance, and then we estimate, by using (1), the TX-RX distance based on the power received.

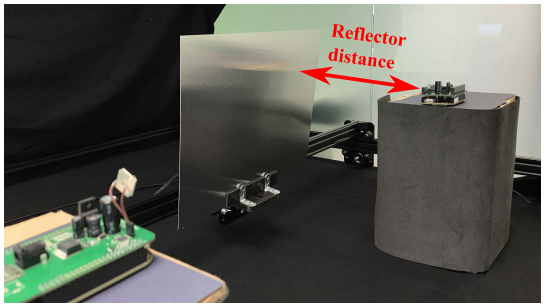

Fig. 2: Testbed.

Figure 3 evaluates the TX-RX distance error with respect to the distance of the reflective material from the LOS link. As expected, the smallest error is obtained when there is only a LOS component (i.e. no reflective material). Depending on the reflective material and its distance, the accuracy of the LPS may change.

B. Basic intuition behind the proposed approach

The detection of NLOS components could be performed in systems with an expensive receiver with high gain-bandwidth product that samples quickly and have enough processing capabilities to compute the CIR [26]. This requires a very high sampling rate at the receiver, which is not feasible in low-end systems.

Instead of computing the CIR, we exploit the fact that, in a dynamic environment, a reflector does not appear suddenly, but enters the illuminated area progressively and the reflections are received by the PD at a certain speed (creating the NLOS component). This phenomenon is represented in Fig. 4[1] that, indeed, is the setup configured in this work for addressing LPS problems in mobile scenarios. Using past data, the receiver first observes an RSS variation due to the transition between the LOS and "LOS+NLOS" conditions and, subsequently, a transition between the "LOS+NLOS" and LOS conditions (when the reflective material is moving away). The shape of the time sequence depends on the material reflecting the light. Note that, as reflections are typically intermittent in vehicular or wearable network scenarios, the system can rely on knowledge of LOS information acquired in a certain time period. Since the first-order reflection may affect the communication and location algorithm [27], the objective of this work is to tackle the localization errors that this NLOS component generates.

C. Testbed

Moving from the realm of theory and simulations into empirical evaluations requires a testbed. We require a testbed with modules capable of providing light-based positioning and

[1]We consider a mobile reflector and static TX and RX, but the same concepts applies to other cases as long as there is a relative movement among TX, RX, and the reflector. For instance, mobile TX and RX, and a static reflector; or mobile TX and RX and a mobile reflector at different speeds.

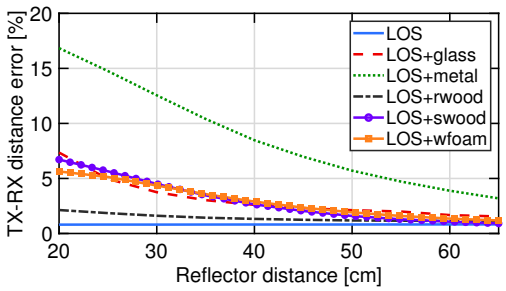

Fig. 3: Experimental TX-RX distance error against reflector distance for multiple materials.

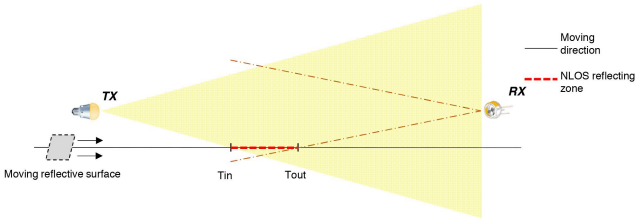

Fig. 4: Schematic representation of reflections in the presence of mobility. The red dashed line depicts the reflecting zone.

mobility. On the one hand, the positioning requirement is addressed by the use of OpenVLC boards for LPS [17]. On the other hand, the mobility requirement is addressed by mounting these boards onto a structure that was originally designed for medium-scale 3D printing: the OpenBuilds ACRO movement structure [28] (see Fig. 2). We bundle these two systems together (mechanically, electrically, and with software) to provide a precisely controlled environment. Our testbed can reproduce fully customizable down-scaled mobile scenarios and automatize the collection of raw data.

Without loss of generality, we move the reflecting materials and keep the positions of the TX and RX fixed (as the movement can be considered relative). The reflective surface is fixed on top of the mobile unit of the system (see Fig. 2), and it can move at a maximum speed of 42 cm/s and a maximum acceleration of 2 m/s^2 per axis. Table I reports the parameters of our testbed. Note that movement between TX and RX is also studied in a following section in order to distinguish reflections from TX-RX relative movements.

All of our experiments use the following setup. The TX and the RX are placed at a distance of 70 cm. The TX emits a fixed light intensity. The RX acquires a trace of 7.5 seconds (i.e. 1.5 million samples) for each movement. To consider various reflector distances, i.e., distances between the LOS path and the reflecting material, we start from a distance of 20 cm, and then move the reflective surface away in steps of 5 cm up to a distance of 65 cm (10 different distances). The same measurement is repeated 30 times in order to have statistical relevance. Thus 300 traces are collected for each material, plus another 300 for the "pure LOS" condition. Although all our experiments are carried out in the darkness, external illumination sources would not affect the system performance due to the fact that reflections still vary over a short time period.

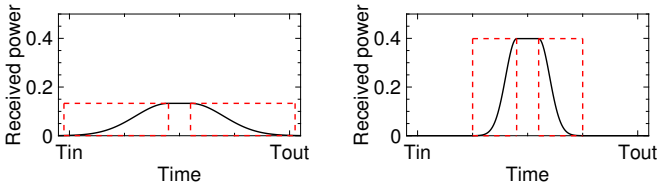

(a) Diffuse object. (b) Specular object.

Fig. 5: Example of power received from reflection over time when diffuse (a) and specular (b) materials moves into an illuminated area.

TABLE I: Testbed parameters.

Parameter	Value
Nodes	2 OpenVLC boards
LED luminous flux	956 lm
LED half-power semi-angle	55°
Single-pixel PD area	7.02 mm^2
Single-pixel PD FOV	120°
Single-pixel PD spectral sensitivity	80 nA/lx
Sampling	12 bits @200 kHz
Movement grid	130 cm x 130 cm

III. Identifying Reflections

As stated in Section II, removing the effects of reflections in LPS implies identifying those reflections and discerning valid RSS changes. In this section, we tackle the identification problem for a series of RSS measurements.

Reflections cause peaks in light intensity, but these peaks can take widely different shapes depending on the properties of the reflecting material. Our first task is to define a minimal set of features to identify all such peaks. When light impinges upon a material, all reflected components are summed-up at the receiver. The final received intensity depends on two key properties: First, the reflection coefficient, i.e., the more reflective the material is (e.g., a mirror), the higher the light intensity reflected; Second, the material smoothness, i.e., a very diffuse material (e.g., white paper) has a wide contribution in space because it reflects light in all directions. This type of materials lead to short but wide reflection peaks, as shown in Fig. 5a. On the other hand, a specular material (e.g. a smooth metallic plate) will only reflect light near the Snell angle [29] that leads to high and narrow peaks as represented in Fig. 5b. Furthermore, the shape of the peaks is also affected by the size of the reflective material, and by their relative speed (bigger materials and slower speeds lead to wider peaks). The number of materials and the variety of sizes and speeds would lead to a large number of peak shapes. To generalize the solution, we need an approach for identifying reflections that is material-, size- and speed-independent:

- Material-independent: The common property in all reflection peaks is that the power received by the NLOS component increases when the reflective object enters the illuminated area, reaches a maximum when the whole material is illuminated and starts decreasing when the material gets out of that area, an action that can be seen in Fig. 4. This effect is represented in Fig. 5, where the received power is plotted for two different reflectors. Note

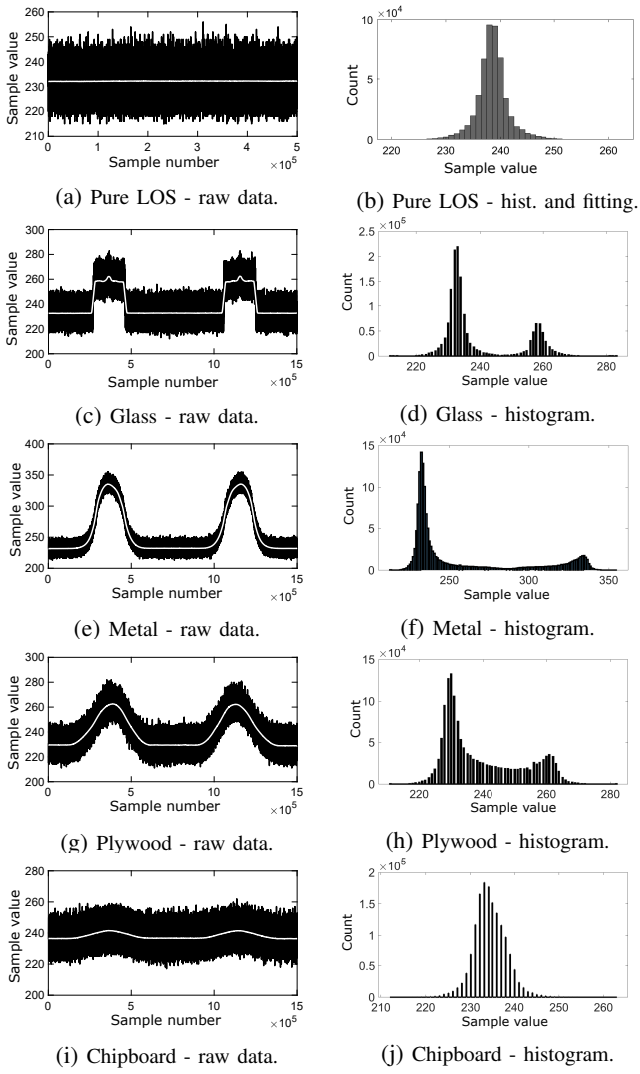

(a) Pure LOS - raw data. (b) Pure LOS - hist. and fitting.

(c) Glass - raw data. (d) Glass - histogram.

(e) Metal - raw data. (f) Metal - histogram.

(g) Plywood - raw data. (h) Plywood - histogram.

(i) Chipboard - raw data. (j) Chipboard - histogram.

Fig. 6: Typical signal for "LOS+NLOS" condition with different reflector materials. Left side: raw data. Right side: histograms.

that the maximum peak and the length of the transitions can change depending on the material, but the shape is similar and useful to identify a NLOS path.

- Size-independent: The plateau of the peak in Fig. 5 is determined by the size of the reflective material. Thus, if the study focuses only on the intrinsic properties of the received signal transitions, that is the upward and downward slopes highlighted in red in Fig. 5, the proposed approach may be considered as size-independent.
- Speed-independent: As long as the sampling rate is high enough compared to the object speed, speed variations will not modify the statistics of the received signal.

Each material and each surface type, due to its unique properties, reflects light differently. This is why this work analyzes different materials, trying to identify the reflection properties that are similar (and different) among them.

A. Statistics considered

Let us consider a "Pure LOS" scenario and four "LOS+NLOS" scenarios composed of materials with distinct reflective features (glass, metal, plywood and chipboard). Using our experimental setup introduced in Section II-C, Fig. 6 shows the raw traces and distributions for these cases. For the "Pure LOS" case (Fig. 6a and 6b), we observe, as expected, a normal distribution with $\mu = 238$ and $\sigma = 2.91$. For the "LOS+NLOS" scenarios (Fig. 6c-6j), we observe peaks that would lead to localization errors. To highlight the behavior hidden underneath the shot and thermal noises, a moving average filtering (white line) is shown. Except for the chipboard, which has a minimal effect due to its weak and diffuse reflection behaviour, all the other materials have bimodal distributions. These bimodal distributions have different trends –for instance, glass produces a sharper reflection than metal or plywood (two well-separated groups of values)–, but all distributions are clearly distinguishable from the "Pure LOS" case.

Our aim is to exploit the peculiar characteristics of the received signal variation over time when light bounces on a given surface. With the constraint of using a given sequence of RSS samples collected with low-cost receivers, here we propose to look at the statistical moments up to the fourth-order as candidate observations to monitor the channel transitions of the NLOS component, and identify those material properties. Apart from the mean μ, and the standard deviation σ, we then consider:

- skewness ($skew$): third-order statistic that gives the amount and direction of skew (departure from horizontal symmetry).
- kurtosis (k): fourth-order statistic that defines how tall and sharp the central peak is, relative to a standard bell curve (i.e. normal distribution where $k = 3$) [30].

Since we are considering low-computational algorithms, higher-order statistics (HOS) are not taken into account because the higher the moment, the harder it is to estimate. Moreover, larger sample intervals are required in order to obtain estimates of similar quality. Finally, due to the high noise power produced when using off-the-shelf devices, HOS are significantly less robust than lower-order statistics.

B. Region of interest (ROI) of the received signal

The detection of the NLOS component in the received signal depends on the statistical properties of the signal itself. As observed previously, the information we want to exploit lies in the transition between LOS and "LOS+NLOS". Therefore, we compute the region of interest (ROI) to select the subset of samples in which we are interested, by searching for changes in the signal [31]. Here, a change in the signal is given by a significant variation of the first statistical moment (i.e. the mean value μ). If μ is considered as a parameter for detecting changes, then a proper algorithm would return the index at which μ changes most significantly (e.g. index corresponding to the blue dashed line of Fig. 7a and Fig. 7d). Instead, if the statistical parameter is the standard deviation σ, the algorithm would return the index relative to the beginning/ending of the rising/falling edge, which is the area where σ changes the most (red dashed line of Fig. 7a and Fig. 7d). As examples

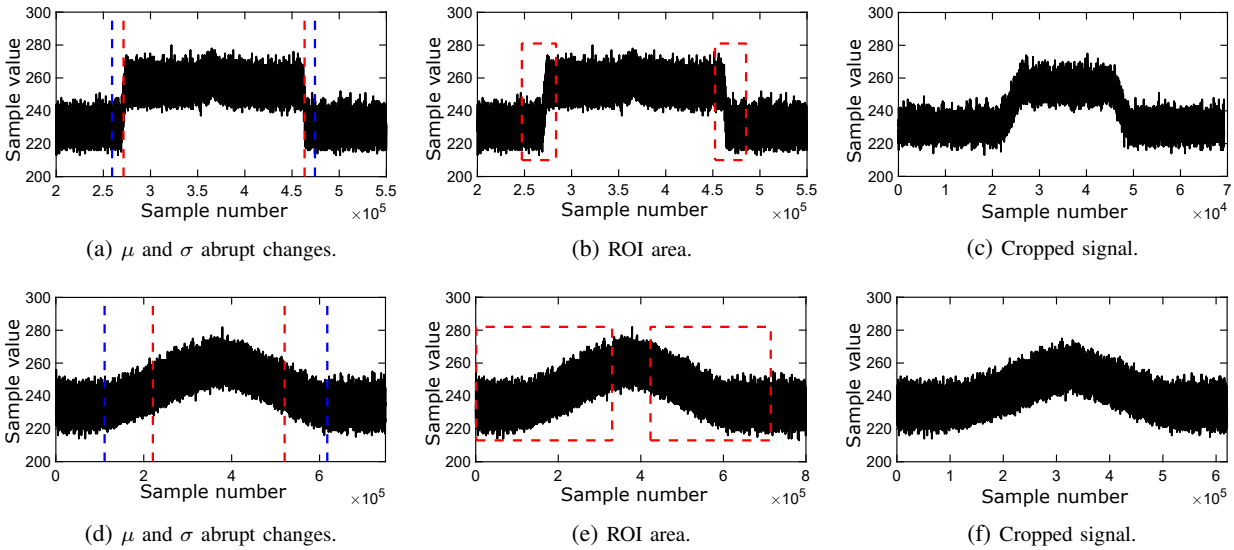

(a) μ and σ abrupt changes. (b) ROI area. (c) Cropped signal.

(d) μ and σ abrupt changes. (e) ROI area. (f) Cropped signal.

Fig. 7: Typical ROI selection steps for glass (a-c) and white foam (d-f).

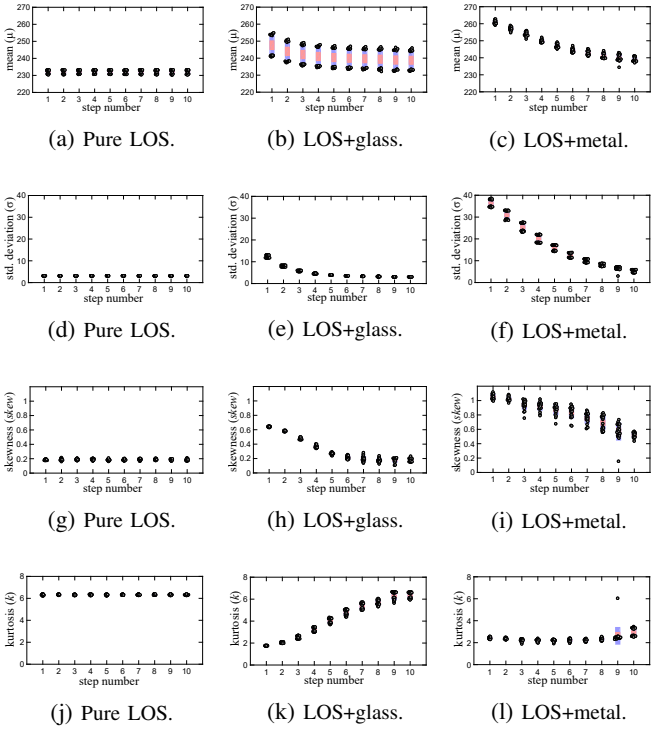

(a) Pure LOS. (b) LOS+glass. (c) LOS+metal.

(d) Pure LOS. (e) LOS+glass. (f) LOS+metal.

(g) Pure LOS. (h) LOS+glass. (i) LOS+metal.

(j) Pure LOS. (k) LOS+glass. (l) LOS+metal.

Fig. 8: Statistical parameters μ (a-c), σ (d-f), skewness (g-i), kurtosis (j-l) against step numbers (i.e., distance to the reflector that goes from 20 to 65 cm in steps of 5 cm). Comparison among "Pure LOS", "LOS+glass" and "LOS+metal" are also represented.

of this procedure, the ROI selection steps for two different materials are shown in Fig. 7. Starting from the whole traces of Fig. 6, the signal is processed for detecting regions of interest[2]. Our algorithm works as follows. First, the signal is filtered with a smoothed filter for removing the noise, allowing a sharp ROI selection. Then the regions between the μ and σ changes, named "transition intervals", are selected. As a final step, in order not to alter the statistical properties of the signal and make the selection size-and-speed-independent, the ROI is extracted by taking the "transition interval" plus the same amount of this interval before and after it as highlighted in Fig. 7b and Fig. 7e. The result is the signals of Fig. 7c and Fig. 7f for glass and white foam, respectively, that will be used for the statistical analysis.

C. Assessment of observables to identify reflections

As we perform a statistical analysis, we show in Fig. 8 the trend of each observable (mean, standard deviation, skewness and kurtosis) over step numbers, which represent the reflector distances from 20 to 65 cm in steps of 5 cm. Note that only values for glass and metal reflectors are discussed, as they are the most representative cases of reflection types and typical materials in vehicular scenarios. By analyzing the results, we note that μ and σ follow the same trend for both sample materials. Their values decay exponentially along the distance and converge to the pure LOS case.

Something more peculiar can be stated for skewness and kurtosis. In the experiment involving glass, skewness tends to the LOS case value more quickly than the values corresponding to the metal case. Glass produces a more directional reflection than metal and only in a determined position along the movement. This is why the NLOS due to glass (specular-like) is lost after a few steps, becoming indistinguishable from noise.

Skewness and kurtosis values for all the scenarios acquired at step number 1 are reported in Table II. Note that the "Pure LOS" condition can be clearly identified by only exploiting skewness and kurtosis. Also, a high-level estimation of different types of reflector materials can be given, leaving space to an in-depth analysis for a material-type classification (i.e. specular-like and diffuse-like material groups), but this is out

[2]With a double passage back and forth, there are two ROIs.

TABLE II: Example values of $skew$ and k for step number 1

Condition	$skew$	k
Pure LOS	0.18	6.32
LOS+metal	1.05	2.41
LOS+swood	0.67	2.08
LOS+glass	0.64	1.77
LOS+wfoam	0.55	2.20
LOS+rwood	0.17	4.92

the scope of this paper and a possible future research line. Besides, note that all the "LOS+NLOS" scenarios tend to look the same and approach the "Pure LOS" condition for larger distances. Therefore, after a certain distance, the identification cannot be performed anymore. However, in those cases, the reflection due to a specific material or large distance leads to a very weak contribution and the generated noise into the system can be considered negligible (refer to Section II-A).

IV. Classification problem proposed

We start this section by solving the problem of discerning valid RSS changes and then introducing a low-cost decision tree algorithm to learn which RSS sequences are caused by reflections.

A. Relative movement of devices

As seen until now, a quick object passage produces a reflection which can lead to a significant amplitude signal variation. As shown in Section II-B a relative linear movement between devices cannot be distinguished easily from the presence of a reflector object. It is necessary to investigate if the statistical methodology proposed in the previous section to detect reflections is still valid in presence of relative movements between the TX and the RX. We want our method to detect reflections when they are present, but not to remove relative movement information, as it will lead to a higher error on the computed location, our final goal. The statistical properties of the received signal are related to the relative speed between TX and RX, and the sampling rate. Thus, if we want to make our metric speed independent, we should look into the number of samples obtained per unit of distance. Two acquisition systems will have the same behavior if the $\frac{speed}{sampling\ rate}$ ratio is the same. Therefore, keeping the number of samples per unit of area constant, the movement of fast objects can be studied by decreasing the sampling rate. In fact, increasing the number of samples per unit of distance does not necessarily lead to a better detector accuracy. A system needs sufficient samples to detect a change in the signal, but sampling the signal more will not improve the detection. Taking this into account, we perform tests at low speeds, so that the experimentation can be correctly performed with a low-sampling-rate device and safely carried out also in an indoor controlled environment, such as the one presented in Section II-C. Note that, if the movement is too fast that cannot be detected, it will not be even appreciated by the localization algorithm.

We acquire a set of relative movements (approaching or moving away TX and RX) at five different speeds. Figure 9 shows four tests performed at different speeds (v1 = 42 cm/s and v2 = 10.6 cm/s). We see that raw data look specular as the reflective object approaches or moves away at the same speed. Skewness assumes positive and negative values with respect to the direction of the movement, but overall both statistical parameters we consider have very similar values to those related to "LOS+NLOS" conditions (Fig. 8). Therefore a way for discriminating the relative movement of devices is needed. By supposing that dynamics change fast in mobile environments, a certain NLOS component may last over a short period of time. An option would be to introduce a time metric, but this would come at the cost of a speed dependent measure, which is undesired. We instead propose a metric that is the sum of the difference between consecutive samples, denoted by the variable

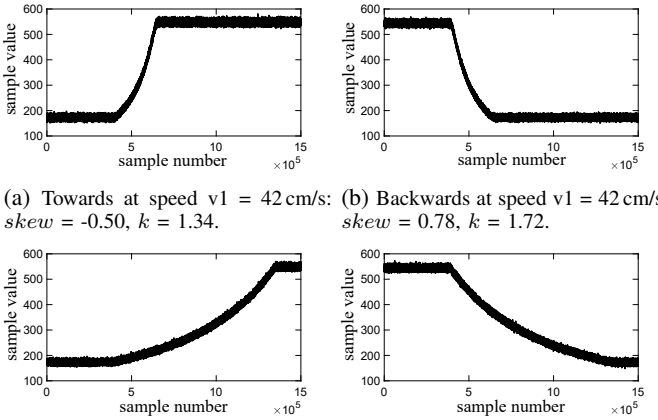

(a) Towards at speed v1 = 42 cm/s: $skew$ = -0.50, k = 1.34.

(b) Backwards at speed v1 = 42 cm/s: $skew$ = 0.78, k = 1.72.

(c) Towards at speed v2 = 10.6 cm/s: $skew$ = 0.82, k = 2.24.

(d) Backwards at speed v2 = 10.6 cm/s: $skew$ = 0.21, k = 1.43.

Fig. 9: Typical received signal for a linear movement towards and backwards the transmitter.

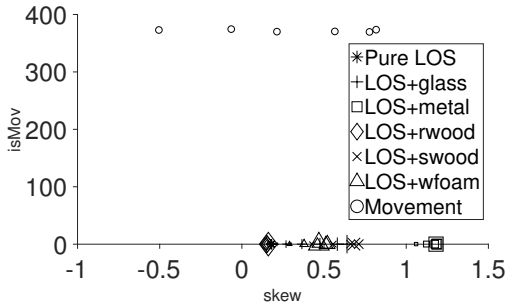

Fig. 10: "isMov" parameter against skewness for different conditions along distances (mean values for each step).

$$isMov = \sum_{i=2}^{N} (x_i - x_{i-1}), \tag{2}$$

where x_i is the i-th sample of the received signal and N is the window signal length. Equation (2) gives us an intuition on how the system is at the end of the measuring window compared to the beginning. If they are very different, the system has changed, otherwise the system relative distance did not change significantly. This lets us distinguish between a signal variation which returns to the same value of the

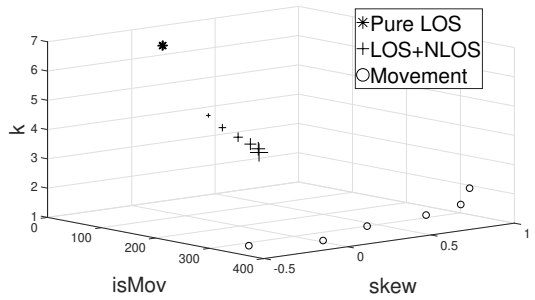

Fig. 11: Scatter plot representing kurtosis, skewness and isMov parameter in case of "Pure LOS", "LOS+NLOS" and "movement".

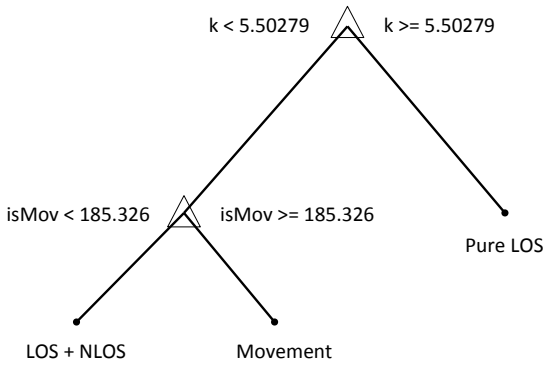

Fig. 12: Coarse tree classification model.

beginning after a fast perturbation (like the one coming from a reflection) and an increased final value. Typical values of "isMov" are high (always above 100) only for relative movements. This avoids the fact that relative movements of devices are confused with a LOS to "LOS+NLOS" transition (see Fig. 10).

B. Detection of NLOS reception

Contrary to the first and second moments, skewness and kurtosis are independent of signal intensity, and they can be efficiently used as features in a classification model where three classes are discerned: "Pure LOS", "LOS+NLOS" and "Movement". Figure 11 represents a scatter plot with axes that are skewness, kurtosis and the "isMov" variable. The "LOS+NLOS" class aggregates all the different materials in our tests. We observe that classes are well separated as the "Pure LOS" and "Movement" persist in a very limited area.

Therefore, we can introduce the algorithm to detect NLOS components in fully dynamic scenarios. In order to classify different scenarios, we choose a supervised machine learning classifier. We introduce a Decision Tree (DT) algorithm to let low-cost devices take advantage of NLOS recognition. In particular, here a coarse tree is used as it has a simple structure, fast prediction speed, small memory usage and low computational cost [32], [33].

The classification model we exploit is shown in Fig. 12. As mentioned before, it is a coarse tree algorithm with only two decision nodes. It uses only kurtosis and "isMov" as predictors since, as demonstrated in Fig. 11, they are sufficient

TABLE III: Confusion matrix, model trained on data set A and tested on data set B.

True condition	Predicted condition: Pure LOS	LOS+NLOS	Movement
Pure LOS	100%	0%	0%
LOS+NLOS	26.8%	73.2%	0%
Movement	0%	0%	100%

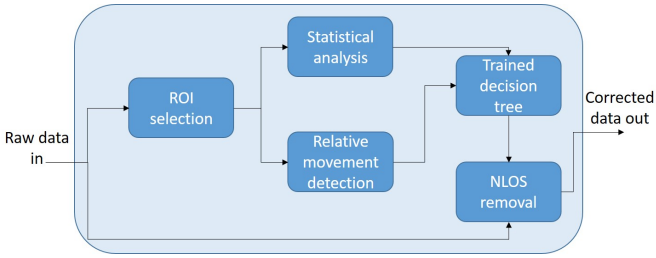

Fig. 13: Block diagram of the algorithm implemented.

for discriminating the three labels (or classes): "Pure LOS", "LOS+NLOS" and "Movement". Skewness would be useful in discriminating a material type from another, but is not the objective of this study.

For training the classification model, we take a data set (A) of 1320 collected observations (200 traces for each LOS and NLOS scenario, considering different step numbers, and 120 for movement). A 5-fold cross validation is employed for avoiding an overfitted training. It has an accuracy of 100%. Finally, for testing the trained classification model, another data set (B) of 660 collected observations (100 for each LOS and NLOS condition, 60 for movement) is used.

Table III shows how the model performs in discerning among classes. In particular, "Pure LOS" and "Movement" are always detected correctly. Differently, the "LOS+NLOS" class suffers the condition in which the NLOS contribution is very poor, and the classification model fails to detect it, with an error of up to 26.8%. Therefore, as expected, there are conditions with low predictive accuracy. Nevertheless, it must be taken into account that the final objective is not simply to detect when there is an object reflecting, but to also remove that reflection.

V. Localization Accuracy Improvement by Removing the NLOS Component

The final goal of this work is to design a method to remove the NLOS components from received VLC signals in order to improve the LPS accuracy. Using the results obtained in Section IV, we design a NLOS removal algorithm. This algorithm detects and corrects the NLOS components that appear in mobile environments.

As input, the algorithm takes the raw data from the ADC. This data is statistically analyzed and the NLOS is detected using the method introduced in Section IV. Then, the NLOS component is removed as follows.

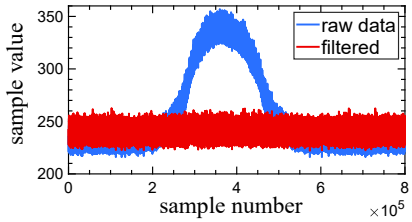

Fig. 14: NLOS removal in a "LOS+metal" condition.

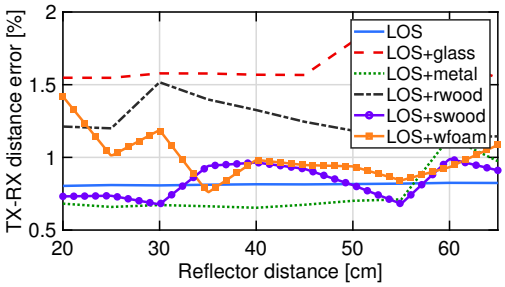

Fig. 15: Distance calculation error after applying correction algorithm (glass = shiny glass, metal = grey satin metal, rwood = chipboard, swood = plywood, wfoam = foam core).

A. NLOS removal

After the signal is received, it is analyzed for detecting the presence of a NLOS component. In order to remove it, the algorithm performs the following steps that are also depicted in Fig. 13:

- First, it detects the ROI where the NLOS component is located. In order to do so, it computes the average value of the whole signal and it detects what part deviates from it. This is selected as the ROI (see Section III-B).
- The ROI is processed by computing the variable "isMov" as (2) indicates in order to determine if there is a relative movement in it. Then it is statistically analyzed using the metrics explained in Section IV.
- The results of this analysis are passed to the trained decision tree, that decides if there is a NLOS component or not.
- If the decision tree decides that a NLOS component is present, it is filtered out from the received signal. This is done by subtracting the ROI average value μ_{ROI} from the ROI and adding the average value of the rest of the received signal μ_{RX}:

$$ROI' = ROI - \mu_{ROI} + \mu_{RX}. \quad (3)$$

The NLOS removal algorithm works only on the ROIs as the rest of the signal is not being filtered. An example of how the algorithm performs is shown in Fig. 14 for a "LOS+metal" condition. As can be seen, the incoming raw data (blue curve) with a significant RSS variation is corrected into a reflectionless signal (red curve) following (3).

B. Algorithm Evaluation

This section analyzes the performance of the NLOS removal algorithm. In particular, using the same data set and the received-power based localization algorithm [17] used in Section II-A, we compute the relative localization of an object using light. The position of the object was computed both with and without the correction algorithm.

TABLE IV: Position accuracy (worst cases)

Condition	W/o correction [cm]	With correction [cm]	Improvement [%]
Pure LOS	0.58	0.58	0
LOS+glass	5.15	1.32	74.3
LOS+metal	11.79	0.8	93.2
LOS+rwood	1.5	1.06	28.8
LOS+swood	4.7	0.7	85.3
LOS+wfoam	3.94	0.99	74.8

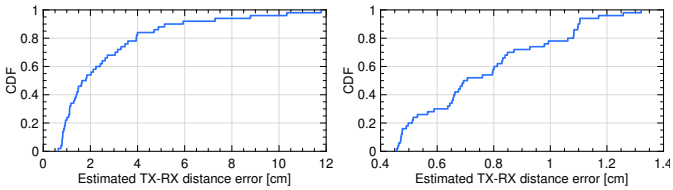

(a) Without correction algorithm. (b) With correction algorithm.

Fig. 16: CDF of the estimated TX-RX distance error. Plots aggregate all the steps and all the conditions.

As it can be seen in Fig. 15, the distance error[3] is always below 2% and the accuracy may increase up to 93% as shown in Table IV. The reason why the error stays low even if the relative power of the NLOS component increases, is that the removal algorithm works better with higher NLOS components. Indeed, when the NLOS component is weak (i.e. the reflective material is far), the ROI selection does not work very well, but the effect on the localization is, as seen in Section II-A (Fig. 3), negligible.

As an additional result, Fig. 16 shows the cumulative distribution function (CDF) of the estimated TX-RX distance error. Note that a significant improvement is achieved when the reflection correction algorithm is used. Indeed, the positioning error can reach a sub-centimeter accuracy with a probability of 80% when filtering is applied.

VI. Related Work

Authors in [10], [16], [21], [22] perform an efficient characterization of the NLOS components to model the CIR. However these solutions come at the cost of high computational resources and the use of specific software even for outdoor applications [34]. Proper countermeasures are then needed for compensating the undesired effect of reflections in VLC [35] and for avoiding the positioning error in LPS [15], [18], [36], [37].

Among other solutions, LOS and NLOS identification algorithms make use of multiple LEDs and PDs [24], [25], [37], which is a condition that may not be available. Some others work opt to use image sensors for cancelling the effect of reflections [4], [5], but it comes with much higher energy consumption cost and lower data rate of communication.

[3]Percent distance error means the positioning error w.r.t. the ground truth, that is fixed and equal to 70 cm.

Our work is an experimental-based analysis and the solution we introduce here exploits a low-cost system allowing a NLOS cancellation in both specular and diffuse reflection conditions. It implies a statistical study of time series of the received signal instead of a way-more-complex and costly CIR estimation. Our method, by using a single-pixel photodetector, offers a solution for overcoming the reflection effect and guaranteeing a better accuracy than more sophisticated systems do.

VII. Conclusion

Motivated by the errors caused by reflections in LPS, this paper presented a new method to filter out multipath components that is suited to be implemented in low-cost positioning receivers that use a single-pixel photodetector. By analyzing the statistical properties of NLOS components and exploiting the results obtained from a custom-built and fully controllable testbed, we have performed an extensive experimental campaign that drove us to design a low-computational cost algorithm to effectively remove the NLOS components, and then to improve the LPS accuracy in up to a 93 %.

References

[1] (2017) LEDs to account for 98% of all lighting by 2025, Frost & Sullivan forecasts. [Online]. Available: https://www.eenewsled.com/news/leds-account-98-all-lighting-2025-frost-sullivan-forecasts

[2] L. Li, P. Hu, C. Peng, G. Shen, and F. Zhao, "Epsilon: A visible light based positioning system," in *Proc. USENIX Symp. on Networked Systems Design and Implementation (NSDI 14)*. Seattle, WA: USENIX Association, 2014, pp. 331–343.

[3] Q. Wang, H. Luo, A. Men, F. Zhao, X. Gao, J. Wei, Y. Zhang, and Y. Huang, "Light positioning: A high-accuracy visible light indoor positioning system based on attitude identification and propagation model," *International Journal of Distributed Sensor Networks*, vol. 14, no. 2, p. 1550147718758263, 2018.

[4] T. Do and M. Yoo, "Visible light communication-based vehicle-to-vehicle tracking using CMOS camera," *IEEE Access*, vol. 7, pp. 7218–7227, 2019.

[5] M. Ratosi and G. Simon, "Real-time localization and tracking using visible light communication," in *Proc. International Conference on Indoor Positioning and Indoor Navigation (IPIN)*, 2018.

[6] Y.-S. Kuo *et al.*, "Luxapose: Indoor positioning with mobile phones and visible light," in *Proc. ACM MobiCom*, 2014.

[7] P. Hu *et al.*, "ColorBars: Increasing data rate of LED-to-camera communication using color shift keying," in *Proc. ACM CoNEXT*, 2015.

[8] R. LiKamWa *et al.*, "Energy characterization and optimization of image sensing toward continuous mobile vision," in *Proc. ACM MobiSys*, 2013.

[9] (2018) Philips indoor positioning. [Online]. Available: http://www.lighting.philips.com/main/systems/lighting-systems/indoor-positioning

[10] W. Gu, M. Aminikashani, P. Deng, and M. Kavehrad, "Impact of multipath reflections on the performance of indoor visible light positioning systems," *J. Lightw. Technol.*, vol. 34, no. 10, pp. 2578–2587, May 2016.

[11] Y. Zhuang, L. Hua, L. Qi, J. Yang, P. Cao, Y. Cao, Y. Wu, J. Thompson, and H. Haas, "A survey of positioning systems using visible LED lights," *IEEE Commun. Surveys Tuts*, vol. 20, no. 3, pp. 1963–1988, thirdquarter 2018.

[12] W. Gu, M. Aminikashani, and M. Kavehrad, "Indoor visible light positioning system with multipath reflection analysis," in *Proc. IEEE International Conference on Consumer Electronics (ICCE)*, Jan. 2016, pp. 89–92.

[13] W. Tang, J. Zhang, B. Chen, Y. Liu, Y. Zuo, S. Liu, and Y. Dai, "Analysis of indoor VLC positioning system with multiple reflections," in *Proc. International Conference on Optical Communications and Networks (ICOCN)*, Aug. 2017, pp. 1–3.

[14] D. Plets, A. Eryildirim, S. Bastiaens, N. Stevens, L. Martens, and W. Joseph, "A performance comparison of different cost functions for RSS-based visible light positioning under the presence of reflections," in *Proc. ACM Workshop on Visible Light Communication Systems (VLCS)*, 2017, p. 37–41.

[15] W. Pan, Y. Hou, and S. Xiao, "Visible light indoor positioning based on camera with specular reflection cancellation," in *Proc. Conference on Lasers and Electro-Optics Pacific Rim (CLEO-PR)*, July 2017, pp. 1–4.

[16] C. Chen, D. A. Basnayaka, X. Wu, and H. Haas, "Efficient analytical calculation of non-line-of-sight channel impulse response in visible light communications," *J. Lightw. Technol.*, vol. 36, no. 9, pp. 1666–1682, May 2018.

[17] A. Galisteo *et al.*, "Follow that light: Leveraging leds for relative two-dimensional localization," in *Proc. ACM CoNEXT*, 2017.

[18] X. Yu *et al.*, "Indoor positioning system based on single LED using symmetrical optical receiver," in *Proc. Asia Communications and Photonics Conference (ACP)*, 2018.

[19] D.-q. Ding and X.-z. Ke, "A new indoor VLC channel model based on reflection," *Optoelectronics Letters*, p. 295–298, Oct. 2010.

[20] Y. Qiu, H.-H. Chen, and W.-X. Meng, "Channel modeling for visible light communications—a survey," *Wireless Communications and Mobile Computing*, vol. 16, no. 14, pp. 2016–2034, 2016.

[21] C. Chen, D. Basnayaka, and H. Haas, "Non-line-of-sight channel impulse response characterisation in visible light communications," in *Proc. IEEE International Conference on Communications (ICC)*, May 2016, pp. 1–6.

[22] N. A. Mohammed and M. A. Elkarim, "Exploring the effect of diffuse reflection on indoor localization systems based on RSSI-VLC," *Opt. Express*, vol. 23, no. 16, pp. 20 297–20 313, Aug. 2015.

[23] M. A. Elkarim, N. A. Mohammed, and M. H. Aly, "Exploring the performance of indoor localization systems based on VLC-RSSI, including the effect of NLOS components using two light-emitting diode lighting systems," *Optical Engineering*, vol. 54, no. 10, pp. 1 – 9, 2015.

[24] C. Huang and X. Zhang, "LOS-NLOS identification algorithm for indoor visible light positioning system," in *Proc. International Symposium on Wireless Personal Multimedia Communications (WPMC)*, Dec. 2017, pp. 575–578.

[25] J. Xu, H. Shen, W. Xu, H. Zhang, and X. You, "LED-assisted three-dimensional indoor positioning for multiphotodiode device interfered by multipath reflections," in *Proc. IEEE Vehicular Technology Conference (VTC Spring)*, June 2017, pp. 1–6.

[26] J. Chen and C. Yan, "A channel model for indoor visible light communication system with specular reflection," in *Proc. International Conference on Optical Communications and Networks (ICOCN)*, Aug. 2017, pp. 1–3.

[27] C. Chen, D. Basnayaka, and H. Haas, "Non-line-of-sight channel impulse response characterisation in visible light communications," in *Proc. IEEE International Conference on Communications (ICC)*, May 2016, pp. 1–6.

[28] (2018) Acro system. [Online]. Available: https://openbuilds.com/builds/openbuilds-acro-system.5416/

[29] M. Fox, *Optical properties of solids (2nd ed.)*. Oxford: Oxford University Press, 2010.

[30] S. Brown, *Measures of Shape: Skewness and Kurtosis*. Oak Road Systems, 2018.

[31] R. Killick, P. Fearnhead, and I. A. Eckley, "Optimal detection of changepoints with a linear computational cost," *Journal of the American Statistical Association*, vol. 107, no. 500, pp. 1590–1598, 2012.

[32] A. Mannini and A. M. Sabatini, "Machine learning methods for classifying human physical activity from on-body accelerometers," *Sensors*, vol. 10, no. 2, pp. 1154–1175, 2010.

[33] D. B. M. Susi and G. Lachapelle, "Accelerometer signal features and classification algorithms for positioning applications," *International Technical Meeting of The Institute of Navigation*, 2011.

[34] S. J. Lee, J. K. Kwon, S. Y. Jung, and Y. H. Kwon, "Simulation modeling of visible light communication channel for automotive applications," in *Proc. International IEEE Conference on Intelligent Transportation Systems*, Sep. 2012, pp. 463–468.

[35] F. Miramirkhani, O. Narmanlioglu, M. Uysal, and E. Panayirci, "A mobile channel model for VLC and application to adaptive system design," *IEEE Commun. Lett.*, vol. 21, no. 5, pp. 1035–1038, May 2017.

[36] H. Huang, L. Feng, P. Guo, A. Yang, and G. Ni, "Iterative positioning algorithm to reduce the impact of diffuse reflection on an indoor visible light positioning system," *Opt. Eng.*, vol. 55, no. 6, pp. 1 – 7, 2016.

[37] S. Shawky *et al.*, "Improved vlc-based indoor positioning system using a regression approach with conventional rss techniques," in *2017 13th International Wireless Communications and Mobile Computing Conference (IWCMC)*, 2017.